

Cite this: *J. Mater. Chem. A*, 2020, **8**, 20054

Pressure-driven significant phonon mode softening and robust superconductivity in layered germanium phosphide†

HPSTAR
1016-2020Jingyan Song,^{‡ab} Ge Fei,^{‡a} Xiaobing Liu,^{‡*a} Shuai Duan,^a Bingchao Yang,^{‡a} Xin Chen,^{‡*a} David J. Singh,^{‡c} Yunxian Liu,^{‡a} Liuxiang Yang,^{*b} Jiangang Guo^{de} and Ping Zhang^{af}

Recent discoveries in high pressure science have revealed entirely unexpected chemical behavior of two-dimensional (2D) materials. However, there is still a lack of unambiguous insight on the pressure-driven behavior of in-plane bonds in the 2D layered structures. Layered germanium phosphide (GeP₅) is a metal with honeycomb-like sheets structurally similar to semiconducting black phosphorus, but with electrical conductivity ten times higher than that of graphite. Here, we report a remarkable pressure-dependent structural transformation that includes lengthening of the main in-plane bonds under pressure, although practically high pressure usually leads to shorter stiffer bonds. *In situ* Raman measurements show that there is significant phonon mode softening through the 2D–3D structural reconstruction, correlating with the in-plane bond extensions in GeP₅ upon compression. This is accompanied by unusually superconducting behavior, on both sides of the transformation. This superconductivity with a maximum transition value of 10.5 K at 13.5 GPa shows a robust character without obvious reduction up to 60 GPa and is accompanied by pressure-induced amorphization in GeP₅. Our experimental results, together with those from first principles calculations, not only provide the detailed high-pressure phase diagram of GeP₅ but also connect the pressure-dependent bond extension with enhanced superconductivity.

Received 24th July 2020
Accepted 19th September 2020

DOI: 10.1039/d0ta07243e

rsc.li/materials-a

1 Introduction

Recent investigations have demonstrated that the structure and intrinsic physical properties of two-dimensional (2D) materials can be extremely sensitive to pressure, leading to the discovery of novel physical and chemical properties by application of external pressure. One recent example is the opening of a sizable 2.5 eV band gap in trilayers of normally gapless graphene under moderate compression,¹ which has severely hampered the practical application of graphene-based transistors,^{2–4} and preservation of this to relatively low-pressure conditions. Semiconducting black phosphorus (BP), which

has a tunable bandgap from ~2.0 eV for monolayer to ~0.3 eV for bulk materials is a buckled honeycomb material that is attracting considerable interest as an emerging 2D material.^{5–10} The high-pressure behavior of BP have been studied, and in particular bulk layered BP has a reversible semiconductor to metallic transition and superconductor upon compression.¹¹ Other examples in layered materials include extremely large magnetoresistance,¹² insulator–metallic transition,^{13–16} large and linear Nernst effect,¹⁷ superconductivity^{18–22} and periodic lattice distortion.²³ Those unexpected discoveries of remarkable physical properties have opened the floodgates to new high-pressure research in novel 2D materials.

Experimental studies and theoretical calculations have indicated that the chemical bonds in layered structures are sensitive to external pressure conditions by effective shortening the atomic spacing to overcome high formation energy barriers. However, there is still a lack of unambiguous insight on the pressure-driven behavior of in-plane bonds in the layered materials, which could allow a comprehensive understating of their 2D–3D structural reconstruction mechanism. Germanium phosphide (GeP₅) is a closely related material with a similar 2D layered structure, that has been shown to be promising for applications including electronics, energy conversion and storage devices.^{24–27} Unlike BP, GeP₅ is metallic at ambient

^aSchool of Physics and Physical Engineering, Qufu Normal University, Qufu, Shandong 273165, China. E-mail: xiaobing.phy@qfnu.edu.cn; chenxin@qfnu.edu.cn^bCenter for High Pressure Science and Technology Advanced Research, Beijing 100094, China. E-mail: liuxiang.yang@hpstar.ac.cn^cDepartment of Physics and Astronomy, University of Missouri, Columbia, MO 665211, USA^dSchool of Physics, University of Chinese Academy of Sciences, Beijing 100094, China^eSongshan Lake Materials Laboratory, Dongguan, Guangdong 523808, China^fInstitute of Applied Physics and Computational Mathematics, Beijing, 71037, China

† Electronic supplementary information (ESI) available. See DOI: 10.1039/d0ta07243e

‡ The authors contributed equally to this work.

pressure. Here we find a remarkable pressure-dependent structural transformation that includes lengthening of the main in-plane bonds under pressure. This is accompanied by unusually robust superconducting behavior, on both sides of the transformation.

High pressure measurements are of necessity more limited than those at ambient pressure. This limits the amount of structural and chemical information that can be obtained. Raman spectroscopy is an important technique for detecting and understanding the structural state of a substance and the effect of changes in interatomic distances on bonding *via* the vibrational spectrum.^{28–32} Measurements of the strain dependence of Raman active phonons thus play important role in revealing precise information of about chemical bonds within and between layers for 2D materials.^{19,23,30} However, due to the lack of high-quality monocrystalline samples, *in situ* Raman measurements for GeP₅ under high pressure have not been reported. The major challenges are the fabrication of high-quality monocrystalline materials by mechanical milling method and the analysis of their unique crystal structure. The reported crystal structure of GeP₅ is similar to BP, but has are randomly occupied by Ge and P atoms in a fixed occupation of Ge = 1/6 and P = 5/6, with a narrow homogeneity range.^{25,27,33} The apparently narrow composition range for the reported GeP₅ metallic phase suggests ordering, at least locally, as opposed to a random alloy, although the nature of this has not been established experimentally. Here we report a thorough study of the phase transition, electronic structures and physical behaviors under high pressure on a high-quality GeP₅ single crystal. We report *in situ* synchrotron X-ray diffraction (XRD), Raman spectra, electrical transport measurements and density functional theory (DFT) calculations. The crystal that we used was synthesized at 2 GPa and 1400 K in a large volume press.

Our results reveal a phase transition at approximately 15 GPa from 2D layered structure to a 3D covalent bonding network. This is accompanied by significant phonon softening as seen in Raman spectroscopy. This softening is attributed to the extension of in-plane P–P bonds in GeP₅. We also observed a reversible superconductivity up to maximum value of 10.5 K at 13.5 GPa. This superconductivity was robust, and remained up to pressures of 60 GPa. Finally, by combining first principles global structure optimization with experiment, we identify ordered structures for both the ambient pressure and high pressure phases of GeP₅ and use them to explain the superconductivity.

2 Experimental section

2.1 Sample synthesis and characterization

GeP₅ single crystals were grown by the temperature gradient method in a cubic high-pressure apparatus (SPD-6 × 3000). This approach has been successfully used in the past for large-size BP³⁴ and diamond single crystal growth.³⁵ We employed high-purity germanium powder (99.999 wt% purity) and phosphorus (99.999 wt% purity) with a mole ratio of 1 : 5.5 as starting materials. After mixture ~1 hour in argon atmosphere at room temperature, the compacted samples were filled in

a hexagonal boron nitride (h-BN) capsule (8 mm in diameter). Magnesium oxide and graphite (8–10 mm in diameter) tubes were used as thermal insulator and heaters, respectively. Each run for sample growth was ~5 minutes at 2 GPa and temperatures of 1273–1500 K. The heating current was slowly decreased down to room temperature in 2 minutes and the applied pressure was released in 1 minute. The produced samples were studied by a high-resolution optical microscope (Leica M205C), scanning electron microscopy (SEM) with energy-dispersive spectroscopy (EDS) (Zeiss Sigma 500), Raman (Horiba, Lab-RAM HR revolution), XRD (X'Pert3 diffractometer with a Cu-K α target) and transmission electron microscopy (TEM) (JEM02100 Plus).

2.2 *In situ* high-pressure experiments

We carried out synchrotron XRD with wavelength of 0.434 Å in a standard diamond anvil cell (DAC) with 300 μ m flat culets using neon as pressure medium. Synchrotron XRD measurements were performed at GSECARS (sector 13BM-C) of Advanced Photon Source, Argonne National Laboratory. Pressure was measured using the ruby fluorescence method. GeP₅ (~50 μ m diameter, ~8–10 μ m thick) was placed into a 160 μ m diameter hole of rhenium gaskets, pre-indented to 30–35 μ m thickness. *In situ* Raman measurements were performed in symmetric DAC with ultralow fluorescence diamonds and ethyl alcohol medium at room temperature. Four series of data were taken for comparison during the high pressure experiments. The 532 nm laser source with ~300 mW output power was used for sample excitation with 30 s counting times. We further characterized the pressure-dependent electrical properties of GeP₅ using four-probe method in a physical property measurement system (PPMS) (Cryogenic Limited, Mini-CFM-5T-25) at temperatures of 300–1.8 K. We used the van der Pauw method for electrical transport measurements on the GeP₅ samples. Pe–Cu cells were used for the resistance experiments. The cubic boron nitride (cBN) powders (300–500 nm in diameter) were employed as pressure medium and insulating material. The pressure was increased by 1–1.5 GPa per step for all the measurements. After high pressure compression, the recovered samples were measured by Raman, SEM and TEM to characterize their structures.

2.3 Simulation and theoretical calculations

Theoretical calculations were performed using CALYPSO (Crystal structure AnaLYsis by Particle Swarm Optimization) prediction methodology^{36,37} merging with *ab initio* total-energy calculations to search for new GeP₅ phases at high pressures. The simulation cell sizes of 1–6 formula unites (f.u.) were adopted at 0–50 GPa with the integral of 10 GPa, and 100 GPa. We performed structural optimization and electronic property calculations within framework of the DFT³⁸ using the Perdew–Burke–Ernzerhof (PBE) generalized gradient approximation (GGA) functional³⁹ by the Vienna *ab initio* Simulation Package (VASP) code.^{40,41} A plane wave energy cutoff of 600 eV and the Monkhorst–Pack *k*-meshes with a grid spacing of $2\pi \times 0.02 \text{ \AA}^{-1}$ were used to ensure all the enthalpy calculations are well

converged within 1 meV per atom. Phonon dispersions and electron–phonon coupling (EPC) calculations were carried out with density functional perturbation theory using the Quantum-ESPRESSO package⁴² with a kinetic energy cutoff of 90 Ry. The superconducting transition temperature T_c was calculated based on the Allen–Dynes modified McMillan equation,^{43–47} considering the typical Coulomb pseudopotential parameters μ^* of 0.1. We additionally performed cross-checks using the general potential linearized augmented planewave (LAPW) method as implemented in the WIEN2k code, which is an all electron method.⁴⁸ The quoted Fermi surface volumes are from these LAPW calculations.

3 Results and discussion

3.1 Experimental synthesis and characterization

GeP₅ has been reported *via* ball milling and *via* high pressure synthesis. We used a temperature gradient growth method under high pressure and high temperature (HPHT) conditions to synthesize a GeP₅ single crystal. In our growth we made monocrystalline GeP₅ samples with high-purity Ge powders and amorphous red P, with a molar ratio of 1 : 5.5 at a pressure of 2 GPa and temperatures of 1273–1500 K. Large bulk 5 mm diameter GeP₅ crystals are obtained in 5 minutes. Fig. 1a shows a typical GeP₅ sample produced by this HPHT method. The produced GeP₅ samples are layered, and were structurally characterized using high-resolution TEM (HRTEM) and the corresponding selected area electron diffraction (SAED) pattern as shown in Fig. 1b and c. The samples show high-quality single crystalline structure. EDS in Fig. 1d gives the atomic ratio of elements Ge : P = 10.08(1) : 55.66(5.52) without detection of any other impurity elements (note that there are also Cu and C signals from the grid used to hold the sample). The EDS elemental mapping analysis (Fig. 1e and f) shows a highly homogeneous elemental distribution of the Ge and P. Electrical

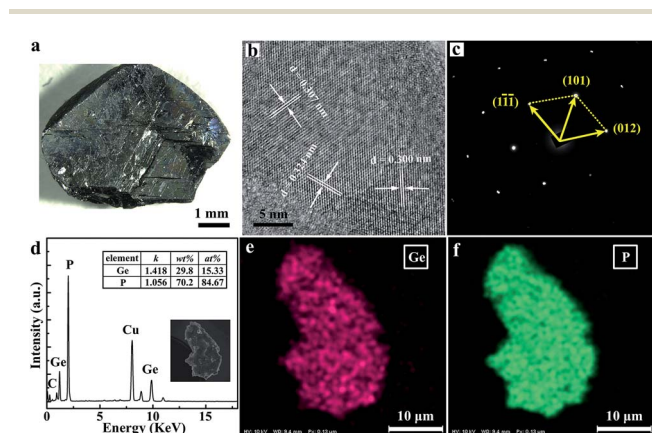


Fig. 1 Structure and characterization of GeP₅ single crystal. (a) Optical image of a produced GeP₅ single crystal at 2 GPa and 1273 K. (b) TEM image and (c) SAED pattern for the grown GeP₅ indicate a high-quality single crystalline structure. (d) Typical EDS data. Cu and C elements in the EDS data are from the TEM substrate. The analyzed composition for the produced sample is close to GeP_{5.52}. Bottom right inset: SEM image of GeP₅. (e) and (f) Represent elemental mapping for Ge and P elements, respectively.

transport measurements for the grown GeP₅ show a metallic character, which persists under pressure as discussed below.

3.2 Significant strain-induced phonon mode softening

We employed *in situ* Raman spectroscopy to study the local structural modifications under pressure of our GeP₅ single crystal (Fig. 2). Two typical Raman peaks with one sharp peak at 429.42 cm⁻¹ and one broad band at approximately 320.47 cm⁻¹ can be identified for GeP₅.²⁶ In our experiment, we pressurized GeP₅ crystal at room temperature up to 60 GPa. Fig. 2a shows the pressure-dependent Raman spectra of a monocrystalline GeP₅ upon compression. We note that the intensity of the dominant sharp peak at 429.42 cm⁻¹ (ω_1) gradually goes down and disappears in the pressure range of 8.83–15.70 GPa, and instead, the intensity of broader 320.47 cm⁻¹ peak (ω_2) is found to increase as the main characteristic peak with increase of pressure through 15.7 GPa. This clearly indicates a structural phase transition (shown in the red dashed box). Additionally, we notice one new peak at lower frequency \sim 300 cm⁻¹ (ω_3) appears at 8.83 GPa, and first it strengthens with pressure increases up to 15.7 GPa, and then it weakens and disappears at pressures above 20.41 GPa. Meanwhile, a broad band at 230 cm⁻¹ (ω_4) and a weak peak at 125 cm⁻¹ (ω_5) appear at 20.41 GPa. At higher pressures above 35 GPa, the Raman spectra is nearly constant, and all the Raman peaks disappear as pressure increases to 60 GPa.

It is striking to observe significant phonon softening of the Raman peaks as the pressure increases, contrary to simple

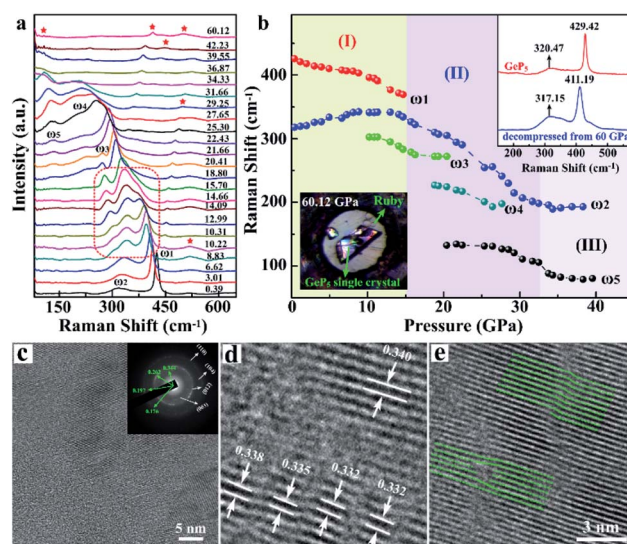


Fig. 2 Strain-induced phonon softening of Raman analysis and amorphous in GeP₅. (a) Selected *in situ* Raman spectra for various pressures up to 60 GPa. The red stars are from the background and ethyl alcohol pressure medium. (b) The measured frequency dependence of Raman-active modes as a function of pressure for GeP₅ single crystal up to 40 GPa. Top right inset: Raman spectrum of the recovered sample after compressed at 60 GPa. Bottom left image is the HP-chamber at pressure of 60.12 GPa. (c) Typical TEM and SAED image for the decompressed GeP₅ from 60 GPa. (d and e) HRTEM images of the recovered GeP₅ sample.

expectations. The pressure dependence of the vibrational frequencies of GeP₅ is summarized in Fig. 2b. The measured wavenumber and shift rates of Raman modes show drastic changes under varying pressure, including three stages: (I) 0–14 GPa, (II) 14–34 GPa and (III) 34–60 GPa. At the first stage, the broad band at 320.47 cm⁻¹ (ω_2) shifts smoothly up to 370 cm⁻¹ at a rate of 1.59 cm⁻¹ per GPa. In contrast, we clearly see that the sharp peak at 429.42 cm⁻¹ (ω_1) exhibits significant red shift down to 400 cm⁻¹. This is at a rate of -3.92 cm⁻¹ per GPa. In second stage (14–20.25 GPa), all the Raman peaks are found to shift down to lower wavenumbers, indicating a rapid phonon softening in the GeP₅ single crystal. At the beginning of the third stage, the sharp peak (ω_3) turns to a broad shoulder at pressure of 27.6 GPa. All the Raman peaks exhibit faster softening throughout the pressure range at rate of 7.24 (ω_2), 3.13 (ω_3), 4.54 (ω_4) and 2.39 (ω_5) cm⁻¹ per GPa. Only a weak shoulder can be found above 100 cm⁻¹ at 34 GPa, while no more detectable features for the GeP₅ exhibits in the Raman spectrum up to 60 GPa. Such significant phonon softening behavior over a large studied pressure range is abnormal. The behavior is in contrast to other 2D materials, such as MoS₂ which also exhibits high pressure superconductivity¹⁹ and SnSe₂, which a high pressure structural distortion.²³ However, a similar phenomenon is reported in solid hydrogen up to 300 GPa.^{28,32} In that system it is due to the weakening of the intramolecular bond accompanied by increased intermolecular interactions.

We observed that the decompressed samples are recovered back to the original states with one sharp peak and one broad band. However, these two peaks of ω_1 and ω_2 have -20 and -3 cm⁻¹ shift, respectively, as shown in the top right inset of Fig. 2b. Meanwhile, a small shoulder around 450 cm⁻¹ can also be noticed in the Raman spectra. This implies a partially irreversible nature to the structural transformation under pressure. The TEM images in Fig. 2c and S1† indicate a pressure-induced amorphization in the decompressed GeP₅ structure above 20 GPa. The remaining crystalline regions in the HRTEM images of the recovered sample show deformation and dislocations (Fig. 2d and e).^{49–53}

3.3 Observation of superconductivity

We performed electrical transport measurements for GeP₅ as a function of pressure. Fig. 3a displays temperature dependence of the electrical resistivity in temperature range of 1.8–300 K at various pressures. We find pressure-dependent superconducting behavior. The resistivity (ρ) decreases from $11.5 \times 10^{-7} \Omega\text{m}$ down to $3 \times 10^{-7} \Omega\text{m}$ at 53.5 GPa with pressure. As the temperature decreases, a sharp drop of $\rho(T)$ is observed for GeP₅, indicating the emergence of a superconducting transition. The critical temperature, T_c is found to be very sensitive to pressure (Fig. 3b), but is robust and persists up to the highest pressure. That is, $T_c = 5.5$ K at 2.5 GPa and increases up to a maximum value of 10.5 K at 13.5 GPa. Following this, the reversible superconductivity remains at ~ 9.5 K up to 60 GPa (Fig. S2a†). In order to confirm the superconducting origin of the resistance drop, we conducted resistivity measurements in the vicinity of T_c under different fields at 13.5 GPa, as shown in

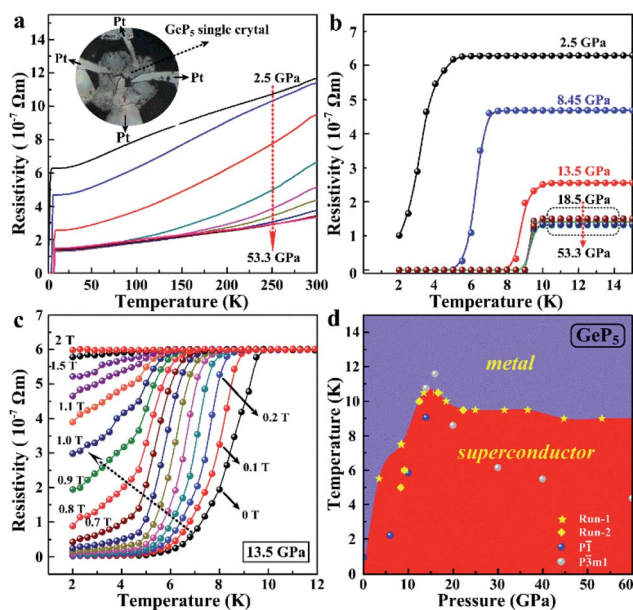


Fig. 3 Transport properties of GeP₅ as a function of pressure. (a) Resistance-pressure curves of ranging from 300 to 1.8 K in the range of 2.5–53.3 GPa. (b) Electrical resistivity as a function of temperature in the range of 1.8–15 K. The error bars for from resistivity measurements are smaller than the symbols size. (c) Temperature dependence of resistivity of GeP₅ under different magnetic fields up to 2 T at 13.5 GPa. (d) GeP₅ electronic phase diagram. The yellow stars and diamonds represent the T_c from various electrical resistance measurements. The error bars for the pressure and resistivity values are smaller than the symbols.

Fig. 3c. The zero-resistance-point is observed to be suppressed with increasing magnetic fields to 2 T. The upper critical field $H_{c2}(T)$ is determined using 90% points on the transition curves. We fitted the data using Ginzburg–Landau theory:

$$H_{c2}(T) = H_{c2}(0) \frac{[1 - (T/T_c)^2]^\alpha}{[1 - (T/T_c)^2]^\beta}$$

yielding a critical field value of 1.4 T for GeP₅.^{22,54,55} The experimental results are summarized in Fig. 3d.

We note that the observed T_c values are similar to those reported for crystalline BP under pressure (6–13 K).¹¹ The superconductivity of BP emerges after a structural phase transition from the orthorhombic ambient pressure semiconducting BP structure, while GeP₅ is already metallic. In addition, one notes that in contrast to previously studied systems,^{22–25,56} such as TMDs, where T_c typically decreases with pressure beyond a maximum value, the superconducting behavior for GeP₅ upon compression, shows remarkable stability up to our maximum pressure of 60 GPa. We also observe that the electrical resistivity at higher temperatures (*e.g.* 300 K) of the recovered GeP₅ sample is much higher than that of the starting material (see Fig. S2b†), while the resistivity is lower at ~ 3 K. These may be related to the pressure-induced amorphization in Fig. 2b or other structural changes as manifested in the phonon shift observed.

3.4 Determination of the phase transition upon compression

We carried out *in situ* synchrotron XRD study for the structure changes up to 40 GPa with a wavelength of 0.434 Å. Typical XRD patterns are shown in Fig. 4a. The diffraction peaks in XRD pattern of GeP₅ under ambient conditions are in excellent agreement with previous studies.²⁵ With increasing pressure up to 12.6 GPa, the in-plane diffraction peaks (003), (104), (105) and (202) broadened, and in particular, the (105) and (113) disappeared. During the compression up to 19.8 GPa, the (003) diffraction peak gradually disappeared and a broad peak was observed (marked as red stars). The (104) peak disappeared at a pressure of 25.4 GPa. Following this, no drastic change was observed to 40 GPa, indicating the stability of structure. Interestingly, we notice that the (101) peak exhibited a red shift starting from the 12.6 GPa up to 40 GPa. The observation of continuous broadening of the in-plane diffraction peaks is in accord with the observed amorphous structure in Fig. 2c–e and S1.†

We performed first-principles structure search calculations at pressures of 0–100 GPa, in order to understand the high-pressure structure, and also to develop a suitable model for low pressure GeP₅ that could be used to understand the superconductivity. The structure search was done using the

swarm-intelligence based CALYPSO structure prediction method.^{36,37} As mentioned, ambient pressure phase is reported as disordered, but likely has at least local order based on the composition. To develop a model, we explored a series of predicted low-enthalpy structures, which are dynamically stable at ambient condition.

According to our calculations in Fig. 4b, the most stable structure for low-pressure conditions is triclinic $P\bar{1}$ that adopts a zigzag puckered structure with alternating Ge–P layers and a honeycomb-like three-coordinated arrangement from the top view (see Fig. S3†). It is important to note that the layered $P\bar{1}$ structure is very similar to rhombohedral BP, except for a lower symmetry in $P\bar{1}$ coming from the ordering of Ge and P in the inner layer. We compared the calculated XRD pattern of the predicted $P\bar{1}$ structure with our experimental measurements in Fig. S3.† This demonstrates that the $P\bar{1}$ structure fits well with experiment. We therefore suggest $P\bar{1}$ structure is a good candidate for the ambient phase, and we use it as our structural model. As shown in Fig. 4b, with increasing pressure, the low-pressure $P\bar{1}$ phase transforms to a new $P\bar{3}m1$ phase at 15 GPa. This remains stable over the whole high pressure range we studied. We notice that the transition pressure coincides well with our experiment (around 13.5 GPa from Raman and electrical transport measurements), and the calculated XRD of high-pressure $P\bar{3}m1$ phase can reproduce almost all the main experimental XRD peaks in Fig. S4,† confirming the transformation of GeP₅ to trigonal $P\bar{3}m1$ symmetry on increasing pressure. The $P\bar{3}m1$ phase stays the most stable structure at pressures up to 60 GPa. No new phase is observed at 40 GPa. Thus the disappearance of Raman phonon features at around 40 GPa (Fig. 2a) can be due to the significant amorphization in GeP₅ structures upon compression (Fig. S1†). Interestingly, the high-pressure structure shows into a P containing part of the unit cell, and a part that has Ge and P. This is quite different from the low-pressure structure, and the kinetics of achieving this separation may relate to the observed pressure-dependent amorphization.

We start with the pressure-dependent chemical bonding changes in the low-pressure GeP₅ $P\bar{1}$ phase. The interlayer Ge–P bond lengths decrease upon compression, as is expected. However, interestingly to find from Fig. 4c that in ambient $P\bar{1}$ structure, the inner-layer P–P bond lengths increase with pressure. This is especially noticeable when the pressure reaches 6 GPa. The extension of inner-layer P–P bonds contributes to the phonon softening that accounts for the experimental observation on the red shift of Raman peak ω_1 , and thus the steep increase of superconductivity in the low-pressure phase of GeP₅, as discussed below. The unusual increase in length, and weakening, of the short and strong in-layer bonds of GeP₅ implies a competition between strong in-layer bonding and weaker inter-layer bonding. This is different from other layered materials, where the weak van der Waals interactions are no match for the strong in-layer bonds. Then, the Raman peak ω_2 can be assigned to Ge–P bond without length shortening in the $P\bar{1}$ phase below 20 GPa.

Related to this, on the basis of the calculated valence electron localization functions (ELF) in Fig. S5,† it is noteworthy that

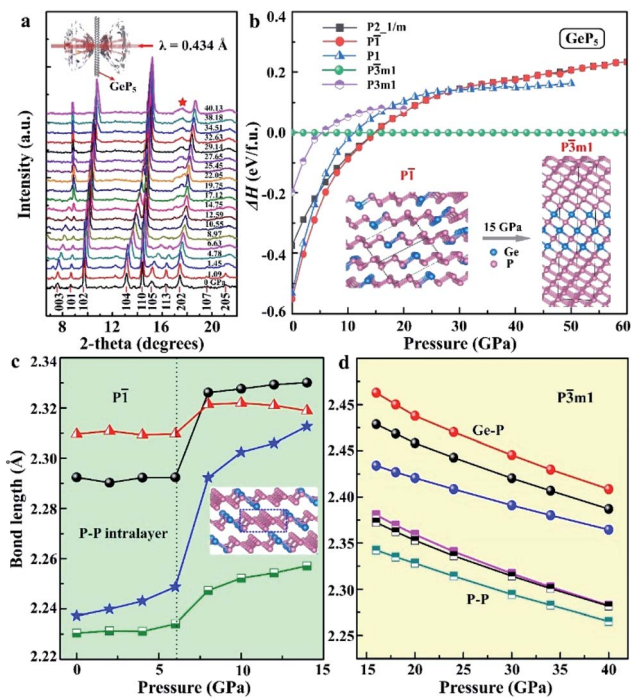


Fig. 4 High-pressure structures of GeP₅. (a) Selected *in situ* synchrotron XRD patterns of GeP₅ sample ($\lambda = 0.434$ Å). (b) Calculated enthalpy curves for predicted structures of GeP₅ relative to $P\bar{3}m1$ phase as a function of pressure. Inset is a diagram of the phase transition from $P\bar{1}$ to $P\bar{3}m1$ structure at 15 GPa. (c) The pressure-dependent change of P–P bond lengths for $P\bar{1}$ structure in the range of 0–14 GPa. The P–P bonds are denoted by the blue dashed rectangle in the inset. (d) The pressure-dependent change of P–P and Ge–P bond lengths for $P\bar{3}m1$ structure in the range of 15–40 GPa.

significantly different from the ambient phase, $P\bar{3}m1$ phase possess a three-dimensional network structure with covalent bonded simple P and Ge-P blocks alternating along c axis (Fig. S3d[†]), in which each Ge/P is coordinated with six P atoms forming edge-sharing octahedral configurations. Thus the high pressure phase arises from three dimensional bonding. Accordingly, in this high pressure phase, Ge-P and P-P bond lengths decrease upon compression, as usual and shown in Fig. 4d. The observed Raman softening (ω_4 and ω_5 above 25 GPa) in experiment is thus from the amorphous structures formed under high pressure (Fig. 2c–e). Moreover, since the appearance and increase of the Raman peaks ω_3 , ω_4 and ω_5 occurs being consistent with the reduction and disappear of the Raman peak ω_1 (interlayer Ge-P bond), it is high likely due to the deformation and reconstruction of P-P bonds the 2D–3D structural transition in the $P\bar{3}m1$ phase under high compression.

3.5 Electronic structure and electron phonon interaction

We used density functional calculations to obtain the pressure-dependent phonons, electronic structure and electron phonon coupling. We begin with the pressure dependence of the phonons. Interestingly, we find from Fig. 5c and d that for the $P\bar{1}$ structure, most phonons with low frequencies harden with pressure; nevertheless, the optical phonon modes obviously soften, especially those between 250 and 350 cm^{-1} along Q – Z – B direction as denoted by the blue dashed rectangle. These phonon modes are dominated by the vibrations of P atoms, which are primarily responsible for the main peak in the

Eliashberg phonon spectral function $\alpha^2F(\omega)/\omega$, and yield an important contribution (of nearly 40% at 10 GPa) to the EPC parameter λ .⁵⁶ The softening of these modes reflects weaker force constants in the layers, as discussed above, and correspond to the longer bond lengths.

The electronic structure near the Fermi level is distinctly three dimensional in character. This is seen in the Fermi surfaces of Fig. 5a and b. This is also the case away from the Fermi level as seen in the band structure of Fig. S6.[†] The three dimensional character of the electronic structure provides an explanation for the unusual structural behavior under pressure. Specifically, it means that electron hopping interactions between layers are not small, and therefore bonding between layers is sufficiently strong to compete with bonding in the layers. Pressure favors this interlayer bonding, and consequently weakens the in-layer bonding. This is analogous to the ultrahigh pressure behavior of hydrogen, where the intramolecular bonds are weakened when the intermolecular interactions are driven up by compression.

There are three bands that cross the Fermi level in GeP_5 at low pressures. Since there are formula units per triclinic unit cell, there is a valence electron deficiency of 2 relative to BP. The three bands crossing the Fermi level lead to three Fermi surface sheets. At ambient pressure, these are a very small hole sheet of volume 0.7% of the zone, a larger hole section of 28.3% of the zone and an open electron section of volume 29.0% of the zone. It is also noted that while similar to BP the electronic structure near the Fermi level comes from p states, unlike BP there is no band gap. There is, however, a dip in the electronic density of states around the Fermi energy. This becomes partially filled in as pressure increases, although a dip remains near the Fermi level. In any case, the changes in electronic structure and phonons with pressure lead to an enhanced λ and superconducting transition temperature T_c (Table S1[†]) that is in accord with the experiment (Fig. 3d). We additionally find that the upon compression, $P\bar{1}$ the electronic structure shows some Fermi surface nesting along Q – Z direction (see Fig. 5b).

As mentioned, GeP_5 remains superconducting through the phase transition. GeP_5 with T_c near 10 K from 20 GPa up to 60 GPa (Fig. 4d). Our calculated T_c for the high-pressure $P\bar{3}m1$ structure is around 11.5 K at 16 GPa, very close to the measurement of 10.5 K. As pressure increases, the calculated T_c reduces slowly, deviating from experiment. Here we suggest this may be caused by the pressure-driven amorphization and deformation in GeP_5 crystals, which is not modeled in our calculations (Fig. 2c–e). Turning to the structure and phonons of the $P\bar{3}m1$ structure, we note that the high-frequency P–P bond vibrations give the main peak of $\alpha^2F(\omega)/\omega$, and produce a high contribution of 70% to λ . As mentioned, the $P\bar{3}m1$ structure consists of a layering of P and Ge–P blocks in the unit cell. Thus, the P blocks in the unit cell, which are metallic due to the electron deficiency in the cell, are important for the superconductivity.

4 Conclusions

In summary, we have comprehensively investigated the pressure-driven behavior in GeP_5 up to 60 GPa by *in situ* Raman

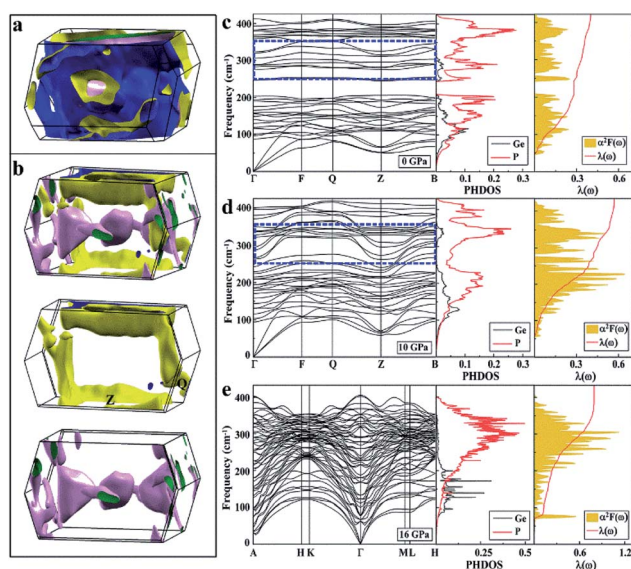


Fig. 5 Calculated electronic and phonon properties. The Fermi surface for $P\bar{1}$ phase of GeP_5 at 0 GPa (a) and 10 GPa (b). The plots in (b) show all three Fermi surfaces and each band crossing the Fermi energy in $P\bar{1}$ structure at 10 GPa, from top to bottom. Calculated phonon dispersions, phonon density of states (PHDOS), the Eliashberg spectral functions $\alpha^2F(\omega)/\omega$, and frequency-dependent electron–phonon coupling parameters $\lambda(\omega)$ for $P\bar{1}$ phase at 0 (c) and 10 GPa (d), and for $P\bar{3}m1$ structure at 16 GPa (e). Blue dashed rectangle in left panel of (c) and (d) shows the softening phonon modes in the $P\bar{1}$ phase upon compression.

spectroscopy, synchrotron XRD, electrical transport measurement and DFT calculations. Our results demonstrate that GeP₅ undergoes a phase transition, $P\bar{1}$ to $P\bar{3}m1$, at approximately 15 GPa from a 2D layered structure to a 3D covalent bonded structure. Both structures have significantly three-dimensional electronic character. This leads to competition between in-layer and inter-layer bonding in the low pressure structure, with resulting unusual bond lengthening under pressure. During the phase transition, we observed the significant phonon mode softening using Raman analysis arising from P-P bonds extension, leading to appearance of a robust superconducting state with maximum T_c value of 10.5 K at 13.5 GPa. The superconductivity persists up to 60 GPa. Our findings not only provide the detailed high-pressure phase diagram of GeP₅, including superconductivity, and provide an example of a layered material with competition between in layer and out-of-layer bonding that is both strong and accessible near ambient pressure.

Author contributions

X. L. designed the study. X. L. and X. C. wrote the manuscript. B. Y. synthesized the samples. J. S. and X. L. conducted Raman, XRD, SEM, TEM, and EDS measurement. L. Y., J. S. and X. L. conducted the synchrotron XRD measurements and analyzed the data. J. S., B. Y., L. Y. and X. L. conducted electrical transport measurement. X. C., G. F., S. D., D. J. S. and Y. L. carried out the first-principles calculations. D. J. S., L. Y., J. G. and P. Z. contributed to provide discussion and helped to prepare the manuscript.

Conflicts of interest

There are no conflicts to declare.

Acknowledgements

This work is supported by the National Natural Science Foundation of China (11974208, 11804184, 11804185, 21905159, 51922105, 51772322 and U1530402), and Shandong Provincial Science Foundation (ZR2019MA054, ZR2019BA010 and ZR2019KJJ020). The calculations were performed in the High-Performance Computing Center (HPCC) of Qufu Normal University. Synchrotron XRD measurements were performed at GSECARS (sector 13BM-C) of Advanced Photon Source, Argonne National Laboratory. Experiments at sector 13BM-C of the APS used the PX² facility, supported by COMPRES under NSF Cooperative Agreement EAR-1606856. Work at the University of Missouri was supported by the U.S. Department of Energy, Basic Energy Sciences, Award DE-SC0019114. X. L. thanks Dr Xiangzhuo Xing at Southeast University for the helpful discussion.

Notes and references

- 1 F. Ke, Y. Chen, K. Yin, J. Yan, H. Zhang, Z. Liu, J. S. Tse, J. Wu, H. K. Mao and B. Chen, *Proc. Natl. Acad. Sci. U. S. A.*, 2019, **116**, 9186–9190.

- 2 L. Ci, L. Song, C. Jin, D. Jariwala, D. Wu, Y. Li, A. Srivastava, Z. F. Wang, K. Storr, L. Balicas, F. Liu and P. Ajayan, *Nat. Mater.*, 2010, **9**, 430–435.
- 3 Y. Zhang, T. T. Tang, C. Girit, Z. Hao, M. C. Martin, A. Zettl, M. F. Crommie, Y. Shen and F. Wang, *Nature*, 2009, **459**, 820–823.
- 4 E. V. Castro, K. S. Novoselov, S. V. Morozov, N. M. R. Peres, J. M. B. Lopes dos Santos, J. Nilsson, F. Guinea, A. K. Geim and A. H. Castro Neto, *Phys. Rev. Lett.*, 2007, **99**, 216802.
- 5 M. Batmunkh, M. Bat-Erdene and J. G. Shapter, *Adv. Mater.*, 2016, **28**, 8586–8617.
- 6 A. Castellanos-Gomez, L. Vicarelli, E. Prada, J. O. Island, K. L. Narasimha-Acharya, S. I. Blanter, D. J. Groenendijk, M. Buscema, G. A. Steele, J. V. Alvarez, H. W. Zandbergen, J. J. Palacios and H. S. J. van der Zant, *2D Materials*, 2014, **1**, 025001.
- 7 J. Qiao, X. Kong, Z. X. Hua, F. Yang and W. Ji, *Nat. Commun.*, 2014, **5**, 4475.
- 8 L. Liang, J. Wang, W. Lin, B. G. Sumpter, V. Meunier and M. Pan, *Nano Lett.*, 2014, **14**, 6400–6406.
- 9 C. Bao and S. Zhou, *Nat. Mater.*, 2020, **19**, 263.
- 10 S. Duan, Y. Cui, X. Chen, W. Yi, Y. Liu and X. Liu, *Adv. Funct. Mater.*, 2019, **29**, 1904346.
- 11 X. Li, J. Sun, P. Shahi, M. Gao, A. H. MacDonald, Y. Uwatoko, T. Xiang, J. B. Goodenough, J. Cheng and J. Zhou, *Proc. Natl. Acad. Sci. U. S. A.*, 2018, **115**, 9935–9940.
- 12 M. N. Ali, J. Xiong, S. Flynn, J. Tao, Q. D. Gibson, L. M. Schoop, T. Liang, N. Haldolaarachchige, M. Hirschberger, N. P. Ong and R. J. Cava, *Nature*, 2014, **514**, 205–208.
- 13 Z. Zhao, H. Zhang, H. Yuan, S. Wang, Y. Lin, Q. Zeng, G. Xu, Z. Liu, G. K. Solanki, K. D. Patel, Y. Cui, H. Y. Hwang and W. L. Mao, *Nat. Commun.*, 2015, **6**, 7312.
- 14 Z. H. Chi, X. M. Zhao, H. Zhang, A. F. Goncharov, S. S. Lobanov, T. Kagayama, M. Sakata and X. J. Chen, *Phys. Rev. Lett.*, 2014, **113**, 036802.
- 15 G. Zhang, Q. Zhang, Q. Hu, B. Wang and W. Yang, *J. Mater. Chem. A*, 2019, **7**, 4019–4025.
- 16 C. Yang, Y. Wang, L. Feng, Q. He, J. Sun, Y. Tang, C. Wu, J. Xiong, W. Zhang, X. Lin, H. Yao, H. Liu, G. Fernandes, J. Xu, J. M. Valles Jr, J. Wang and Y. Li, *Science*, 2019, **366**, 1505–1509.
- 17 Z. Zhu, X. Lin, J. Liu, B. Fauqué, Q. Tao, C. Yang, Y. Shi and K. Behnia, *Phys. Rev. Lett.*, 2015, **114**, 176601.
- 18 Y. Qi, P. G. Naumov, M. N. Ali, C. R. Rajamathi, W. Schnelle, O. Barkalov, M. Hanfland, S. C. Wu, C. Shekhar, Y. Sun, V. Süß, M. Schmidt, U. Schwarz, E. Pippel, P. Werner, R. Hillebrand, T. Förster, E. Kampert, S. Parkin, R. J. Cava, C. Felser, B. Yan and S. A. Medvedev, *Nat. Commun.*, 2016, **7**, 11038.
- 19 Z. Chi, X. Chen, F. Yen, F. Peng, Y. Zhou, J. Zhu, Y. Zhang, X. Liu, C. Lin, S. Chu, Y. Li, J. Zhao, T. Kagayama, Y. Ma and Z. Yang, *Phys. Rev. Lett.*, 2018, **120**, 037002.
- 20 Y. Fu, E. Liu, H. Yuan, P. Tang, B. Lian, G. Xu, J. Zeng, Z. Chen, Y. Wang, W. Zhou, K. Xu, A. Gao, C. Pan, M. Wang, B. Wang, S. C. Zhang, Y. Cui, H. Y. Hwang and F. Miao, *npj Quantum Mater.*, 2017, **2**, 52.

- 21 B. Sipos, A. F. Kusmartseva, A. Akrap, H. Berger, L. Forró and E. Tutiš, *Nat. Mater.*, 2008, **7**, 960–965.
- 22 X. C. Pan, X. Chen, H. Liu, Y. Feng, Z. Wei, Y. Zhou, Z. Chi, L. Pi, F. Yen, F. Song, X. Wan, Z. Yang, B. Wang, G. Wang and Y. Zhang, *Nat. Commun.*, 2015, **6**, 7805.
- 23 J. Ying, H. Paudyal, C. Heil, X. J. Chen, V. V. Struzhkin and E. R. Margine, *Phys. Rev. Lett.*, 2018, **121**, 027003.
- 24 B. Yang, A. Nie, Y. Chang, Y. Cheng, F. Wen, J. Xiang, L. li, Z. Liu and Y. Tian, *J. Mater. Chem. A*, 2018, **6**, 19409–19416.
- 25 W. Li, H. Li, Z. Lu, L. Gan, L. Ke, T. Zhai and H. Zhou, *Energy Environ. Sci.*, 2015, **8**, 3629–3636.
- 26 J. He, Y. Wei, L. Hu, H. Li and T. Zhai, *Front. Chem.*, 2018, **6**, 21.
- 27 W. Li, L. Ke, Y. Wei, S. Guo, L. Gan, H. Li, T. Zhai and H. Zhou, *J. Mater. Chem. A*, 2017, **5**, 4413–4420.
- 28 M. I. Eremets, A. P. Drozdov, P. P. Kong and H. Wang, *Nat. Phys.*, 2019, **15**, 1246–1249.
- 29 Y. Lee, G. He, A. J. Akey, R. Si, M. Flytzani-Stephanopoulos and I. P. Herman, *J. Am. Chem. Soc.*, 2011, **133**, 12952–12955.
- 30 M. Huang, H. Yan, C. Chen, D. Song, T. F. Heinz and J. Hone, *Proc. Natl. Acad. Sci. U. S. A.*, 2009, **106**, 7304–7308.
- 31 M. Granath, J. Bielecki, J. Holmlund and L. Börjesson, *Phys. Rev. B: Condens. Matter Mater. Phys.*, 2009, **79**, 235103.
- 32 X. Huang, F. Li, Y. Huang, G. Wu, X. Li, Q. Zhou, B. Liu and T. Cui, *Chin. Phys. B*, 2015, **25**, 037401.
- 33 P. C. Donohue and H. S. Young, *J. Solid State Chem.*, 1970, **1**(2), 143.
- 34 B. Yang, B. Wan, Q. Zhou, Y. Wang, W. Hu, W. Lv, Q. Chen, Z. Zeng, F. Wen, J. Xiang, S. Yuan, J. Wang, B. Zhang, W. Wang, J. Zhang, B. Xu, Z. Zhao, Y. Tian and Z. Liu, *Adv. Mater.*, 2016, **28**, 9408–9415.
- 35 X. Liu, X. Chen, D. J. Singh, R. A. Stern, J. Wu, S. Petitgirard, C. R. Bina and S. D. Jacobsen, *Proc. Natl. Acad. Sci. U. S. A.*, 2019, **116**, 7703–7711.
- 36 Y. Wang, J. Lv, L. Zhu and Y. Ma, *Phys. Rev. B: Condens. Matter Mater. Phys.*, 2010, **82**, 094116.
- 37 Y. Wang, J. Lv, L. Zhu and Y. Ma, *Comput. Phys. Commun.*, 2012, **183**, 2063–2070.
- 38 L. J. Sham and M. Schlüter, *Phys. Rev. Lett.*, 1983, **51**, 1888.
- 39 J. P. Perdew, K. Burke and M. Ernzerhof, *Phys. Rev. Lett.*, 1996, **77**, 3865.
- 40 J. Furthmüller, J. Hafner and G. Kresse, *Phys. Rev. B: Condens. Matter Mater. Phys.*, 1994, **50**, 15606.
- 41 M. C. Payne, M. P. Teter, D. C. Allan, T. A. Arias and J. D. Joannopoulos, *Rev. Mod. Phys.*, 1992, **64**, 1045.
- 42 P. Giannozzi, S. Baroni, N. Bonini, M. Calandra, R. Car, C. Cavazzoni, D. Ceresoli, G. L. Chiarotti, M. Cococcioni, I. Dabo, A. D. Corso, S. d. Gironcoli, S. Fabris, G. Fratesi, R. Gebauer, U. Gerstmann, C. Gougoussis, A. Kokalj, M. Lazzeri, L. Martin-Samos, N. Marzari, F. Mauri, R. Mazzarello, S. Paolini, A. Pasquarello, L. Paulatto, C. Sbraccia, S. Scandolo, G. Sclauzero, A. P. Seitsonen, A. Smogunov, P. Umari and R. M. Wentzcovitch, *J. Phys.: Condens. Matter*, 2009, **21**, 395502.
- 43 P. B. Allen and R. C. Dynes, *Phys. Rev. B: Solid State*, 1975, **12**, 905.
- 44 L. N. Oliveira, E. K. U. Gross and W. Kohn, *Phys. Rev. Lett.*, 1988, **60**, 2430.
- 45 M. Lüders, M. A. L. Marques, N. N. Lathiotakis, A. Floris, G. Profeta, L. Fast, A. Continenza, S. Massidda and E. K. U. Gross, *Phys. Rev. B: Condens. Matter Mater. Phys.*, 2005, **72**, 024545.
- 46 M. A. L. Marques, M. Lüders, N. N. Lathiotakis, G. Profeta, A. Floris, L. Fast, A. Continenza, E. K. U. Gross and S. Massidda, *Phys. Rev. B: Condens. Matter Mater. Phys.*, 2005, **72**, 024546.
- 47 J. Guo, H. Wang, F. v. Rohr, W. Yi, Y. Zhou, Z. Wang, S. Cai, S. Zhang, X. Li, Y. Li, J. Liu, K. Yang, A. Li, S. Jiang, Q. Wu, T. Xiang, R. J. Cava and L. Sun, *Phys. Rev. B*, 2017, **96**, 224513.
- 48 P. Garbacz, *J. Chem. Phys.*, 2020, **152**, 037101.
- 49 Y. Huang, Y. He, H. Sheng, X. Lu, H. Dong, S. Samanta, H. Dong, X. Li, D. Y. Kim, H. K. Mao, Y. Liu, H. Li, H. Li and L. Wang, *Natl. Sci. Rev.*, 2019, **6**, 239–246.
- 50 L. Wang, B. Liu, H. Li, W. Yang, Y. Ding, S. V. Sinogeikin, Y. Meng, Z. Liu, X. C. Zeng and W. L. Mao, *Science*, 2012, **337**, 825–828.
- 51 Y. Wang, J. Zhu, W. Yang, T. Wen, M. Pravica, Z. Liu, M. Hou, Y. Fei, L. Kang, Z. Lin, C. Jin and Y. Zhao, *Nat. Commun.*, 2016, **7**, 12214.
- 52 X. Yang, M. Yao, X. Wu, S. Liu, S. Chen, K. Yang, R. Liu, T. Cui, B. Sundqvist and B. Liu, *Phys. Rev. Lett.*, 2017, **118**, 245701.
- 53 M. Yao, W. Cui, M. Du, J. Xiao, X. Yang, S. Liu, R. Liu, F. Wang, T. Cui, B. Sundqvist and B. Liu, *Adv. Mater.*, 2015, **27**, 3962–3968.
- 54 Y. Li, E. Wang, X. Zhu and H. Wen, *Phys. Rev. B*, 2017, **95**, 024510.
- 55 E. Wang, X. Zhu and H. Wen, *EPL*, 2016, **115**, 27007.
- 56 P. Garbacz, *J. Chem. Phys.*, 2020, **152**, 037101.